Front. Chem. Sci. Eng. 2021, 15(4): 892–901
https://doi.org/10.1007/s11705-020-2011-0

RESEARCH ARTICLE

Novel Ag-AgBr decorated composite membrane for dye rejection and photodegradation under visible light

Yixing Wang, Liheng Dai, Kai Qu, Lu Qin, Linzhou Zhuang, Hu Yang, Zhi Xu (✉)

State Key Laboratory of Chemical Engineering, School of Chemical Engineering, East China University of Science and Technology, Shanghai 200237, China

© Higher Education Press 2021

Abstract Photocatalytic membranes have received increasing attention due to their excellent separation and photodegradation of organic contaminants in wastewater. Herein, we bound Ag-AgBr nanoparticles onto a synthesized polyacrylonitrile-ethanolamine (PAN-ETA) membrane with the aid of a chitosan (CS)-TiO_2 layer via vacuum filtration and *in-situ* partial reduction. The introduction of the CS-TiO_2 layer improved surface hydrophilicity and provided attachment sites for the Ag-AgBr nanoparticles. The PAN-ETA/CS-TiO_2/Ag-AgBr photocatalytic membranes showed a relatively high water permeation flux (~ 47 $L \cdot m^{-2} \cdot h^{-1} \cdot bar^{-1}$) and dyes rejection (methyl orange: 88.22%; congo red: 95%; methyl blue: 97.41%; rose bengal: 99.98%). Additionally, the composite membranes exhibited potential long-term stability for dye/salt separation (dye rejection: ~97%; salt rejection: ~6.5%). Moreover, the methylene blue and rhodamine B solutions (20 mL, 10 $mg \cdot L^{-1}$) were degraded approximately 90.75% and 96.81% in batch mode via the synthesized photocatalytic membranes under visible light irradiation for 30 min. This study provides a feasible method for the combination of polymeric membranes and inorganic catalytic materials.

Keywords Ag-AgBr, dye rejection, photodegradation, visible light

1 Introduction

Various organic dyes are widely used in textile, painting, printing, pharmaceutical, rubber, cosmetics, and food industries [1–3]. Along with the development of these industries, the treatment of dyes wastewater is becoming increasingly difficult. Due to the toxicity, carcinogenicity, and mutagenicity of dyes, even a small amount can cause severe environmental damages and jeopardize human health [3,4]. Many methods, such as ion exchange [5], chemical coagulation/flocculation [6], chemical oxidation [7], membrane separation [8,9], adsorption [10], photocatalytic degradation [3,11] and electrochemical method [12], have been proposed and developed to remove dyes in wastewater. Among these methods, membrane separation, one of the most applicable and promising techniques to treat dye wastewater, is attractive due to its convenient operation, high efficiency and low energy requirement [13,14].

However, membrane fouling, resulting from the non-specific interaction between organic dyes and the membrane surface [15], could cause decreased separation efficiency, cutting membrane life and increasing energy consumption [16,17]. Usually, hydrophilic modification may be an effective way to improve the antifouling property of membranes [18]. In recent years, photocatalytic membrane has received increasing attention, which combines photocatalyst and membrane for dealing with organic contaminants in wastewater [14,19–25]. Hydrophilic photocatalysts can mitigate the inherent membrane fouling owing to the hydrophilicity and the efficient photocatalytic decomposition of pollutants [16].

In the past decades, TiO_2 has been widely used in the fabrication of photocatalytic membranes [13,16,22–24,26,27]. However, the wide band gap and low sunlight utilization efficiency have confined its practical applications [28–30]. Since 2008, Ag-AgX (X = Cl, Br, I) has been proven to photodegrade the organic pollutants of wastewater outstandingly owing to its superior visible-light activity [30,31]. However, it is very difficult to form a stable catalytic layer on the membrane surface. In order to obtain the best performance of catalysts, the nanoparticles anchored on the membrane surfaces should be exposed to the environment. Several strategies have been reported,

Received July 27, 2020; accepted September 7, 2020

E-mail: zhixu@ecust.edu.cn

including self-assembly [32], epitaxial growth [33], entrapment [34], and chemical binding [35]. Chitosan (CS), linear polymer, possesses outstanding hydrophilicity due to its hydroxyl and amino groups [36]. It can fix TiO_2 nanoparticles on the membrane surface to take advantage of the large specific surface area of TiO_2, which can facilitate catalysts to immobilize on the membrane surface.

Herein, for dye removal and photodegradation, we report a method to bind Ag-AgBr photocatalyst on the CS-TiO_2 layer of PAN-ETA membranes (Scheme 1). First, CS modified TiO_2 was firmly immobilized onto the PAN-ETA membrane surface by a simple vacuum filtration method. The CS-TiO_2 layer is not only used as the dye separation layer, but also provides adhesion site for silver nitrate ($AgNO_3$) [13,33]. Then, Ag-AgBr nanoparticles were formed, via *in-situ* partial reduction onto the CS-TiO_2 layer, to improve the separation efficiency of various dyes. Furthermore, the PAN-ETA/CS-TiO_2/Ag-AgBr membranes showed excellent degradation performance in dye solutions under visible light irradiation, which shows potential in the performances of anti-fouling, self-cleaning, and recyclable stability.

2 Experimental

2.1 Materials and chemicals

Polyacrylonitrile powder (PAN, molecular weight: ~150000) was obtained from Shanghai Jinshan Petroleum. Dimethyl sulfoxide (DMSO, AR, 99%) and absolute ethanol (AR, 99.7%) were purchased from Sinopharm Chemical Reagent Co., Ltd. Ethanolamine (ETA, AR, 99%) was acquired from Shanghai Lingfeng Chemical Reagent Co., Ltd. Silver nitrate (AR, 99.8%), sodium bromide (AR, 99%), glutaraldehyde (GA, RG, 50 wt-% in water), CS and acetic acid (AR, 99.5%) were provided by Adamas Reagent Co., Ltd. Methyl blue (MB, AR), methyl orange (MO, 85%), congo red (CR, ⩾35%), rose bengal (RB, 95%), methylene blue (MEB, ⩾70%) and rhodamine B (RhB, ⩾97%) were purchased from Aladdin Chemical Co., Ltd., China. Titanium dioxide (5 nm) was purchased from Jing Rui New Material Co., Ltd. Deionized water was prepared using a two-stage reverse osmosis process. All chemicals were used as received without further purification.

2.2 Fabrication of PAN-ETA/CS-TiO_2/Ag-AgBr membrane

2.2.1 Preparation of PAN-ETA membrane

PAN-ETA membrane was prepared by a modified *in-situ* polymerization/NIPS method according to our previous work [37]. In detail, 3.6 g of ETA (containing 1% water) and 10.8 g of PAN were added into 45.6 g of DMSO solution and the mixture was then stirred at 80 °C for 8 h. After cooling to room temperature and degassing, the solution was cast on a glass plate and immersed into deionized water to obtain PAN-ETA membranes.

2.2.2 Preparation of PAN-ETA/CS-TiO_2 membrane

TiO_2 (0.1 g) was dispersed in 2 wt-% acetic acid aqueous solution (100 mL) and the solution was ultrasonicated for 1 h, followed by the addition of CS (0.2 g) to form a CS-TiO_2 dispersion. The CS-TiO_2 coating layer was obtained through simple vacuum filtration of the above-dispersed

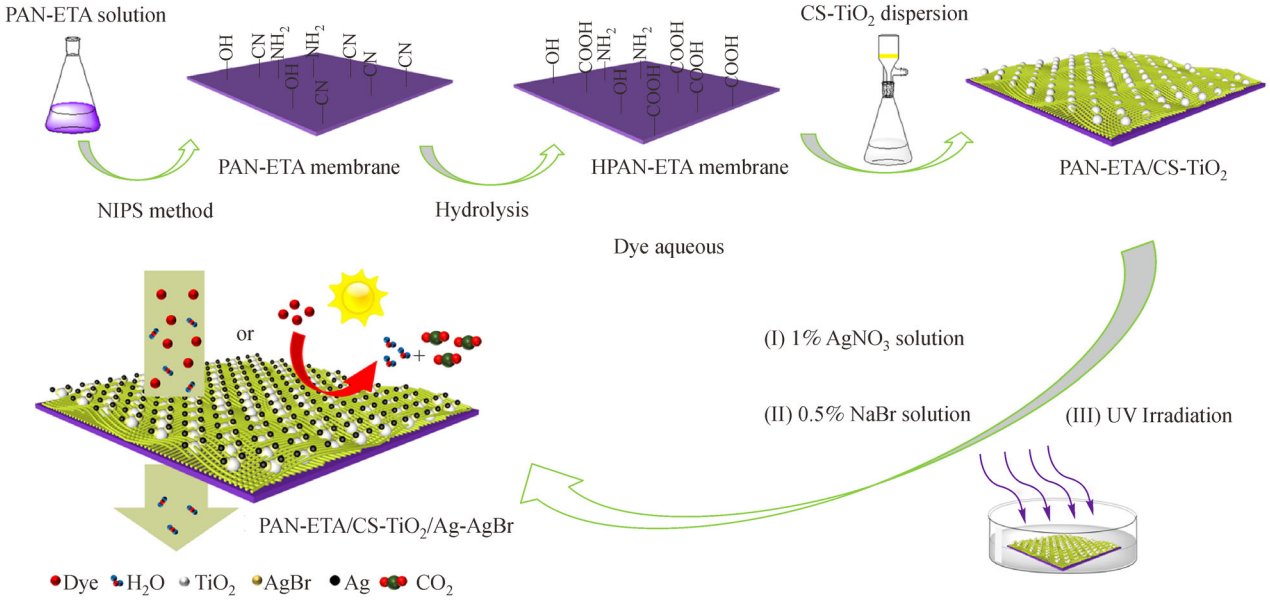

Scheme 1 Schematic for the fabrication of PAN-ETA/CS-TiO_2/Ag-AgBr membrane.

solution and subsequently crosslinked in 1 wt-% GA aqueous solution to fabricate PAN-ETA/CS-TiO_2 membrane.

2.2.3 Preparation of PAN-ETA/CS-TiO_2/Ag-AgBr membrane

CS-TiO_2 modified membrane was immersed into 50 mL of 1 wt-% $AgNO_3$ solution under dark conditions for a designated time to ensure desorption/sorption equilibrium. After rinsing with deionized deionized water, the membrane was immersed into 0.5 wt-% NaBr solution to form AgBr nanoparticles. Then, the above membrane was submerged in deionized water/EtOH solution and irradiated by a 300 W Hg lamp for 10 min to partly decompose AgBr to Ag [30,38]. Finally, the PAN-ETA/CS-TiO_2/Ag-AgBr membrane was stored in deionized water prior to use.

2.3 Characterization

The morphology of the prepared membranes was characterized by field emission scanning electron microscopy (FE-SEM, Nova Nano SEM 450, Japan). To obtain the cross-section, a dry membrane was immersed in liquid nitrogen and fractured, and the fractured surface was sputtered with a thin layer of gold prior to SEM analysis. The chemical components of the modified membranes were analysed by X-ray photoelectron spectroscopy (XPS, VG Microlab II, UK). Attenuated total internal reflectance Fourier transform infrared spectra (ATR-FTIR) of the membrane were recorded on Perkin-Elmer 16 PC FTIR. The contact angle measurement of the dry membrane was done by the sessile drop method using a drop shape analysis system (JC2000A, Shanghai Zhongchen Digital Equipment Co. Ltd., China). The dye concentration was measured by UV-vis spectrophotometer (Shimadzu, UV-2600).

2.4 Dye filtration performance

A self-made cross-flow cell (effective area ~28.26 cm^2) was used to evaluate the pure water flux (PWF) (J) and dye rejection (R) of the as-prepared membranes. Four types of dyes, i.e., MB, MO, VB, and CR, were tested. The dye concentration was fixed at 100 $mg \cdot L^{-1}$, if it is not specially indicated. The membrane was pressurized with deionized water at 0.1 MPa for 30 min before the measurement. The permeate flux (J) was calculated by Eq. (1):

$$J = \frac{Q}{A \times t}, \tag{1}$$

where Q is the volume of permeated water (L), A is the membrane area (m^2), and t is the permeation time (h). Dye rejection (R) was calculated based on Eq. (2):

$$R = \frac{c_f - c_p}{c_f} \times 100\%, \tag{2}$$

where C_f and C_p are the dye concentrations ($mg \cdot L^{-1}$) in the feed and permeate solution, respectively.

2.5 Photocatalysis performance

MEB and RhB were chosen to evaluate the photocatalytic activity of the as-prepared membrane due to its negligible photosensitizing effect under visible light. Typically, the PAN-ETA/CS-TiO_2/Ag-AgBr membrane was cut into small sectors. In order to ensure the desorption/sorption equilibrium, the membrane was immersed into MEB or RhB solution (10 $mg \cdot L^{-1}$) for 30 min under a dark environment. The photocatalytic degradation of MEB or RhB was carried out under continuous stirring in a UV-visible irradiator equipped with a 500 W Xe lamp and a UV cut-off filter ($\lambda > 420$ nm). During photodegradation, 1 mL of the dye solution was gathered at 5 min intervals, followed by UV-vis spectrophotometry to measure the absorbance.

3 Results and discussion

3.1 Characterization of PAN-ETA and composite membranes

The surface morphologies of the as-prepared membranes are shown in Fig. 1. A relatively smooth surface could be clearly found on the PAN-ETA membrane (Fig. 1(a)) and a homogeneous distribution of nanoparticles on the surface demonstrated the successful loading of CS-TiO_2 on the PAN-ETA membrane (Fig. 1(b)). The stable attachment of TiO_2 is mainly attributed to the adhesion effect of CS intertwining networks on TiO_2 nanoparticles. Furthermore, CS with abundant positively charged amine groups could be firmly immobilized onto the negatively charged surface (–COOH and –OH) of hydrolysed PAN-ETA membrane through electrostatic interaction. Figure 1(c) shows the surface morphology of a large number of nanoparticles decorating membrane. We found that small Ag nanoparticles were epitaxially grown on the surface of AgBr nanoparticles.

The XRD patterns and ATR-FTIR spectra of the as-prepared membranes are demonstrated in Fig. 2. In Fig. 2(a), the sharp peaks at 2θ values of 17.3° confirmed the crystalline nature of PAN-ETA. Compared to PAN-ETA membrane, no characteristic peak for crystalline phase was found in PAN-ETA/CS-TiO_2 due to the low exposure of TiO_2 nanoparticles wrapped by CS. For the PAN-ETA/CS-TiO_2/Ag-AgBr membrane, the diffraction peaks of Ag and AgBr simultaneously appears, indicating the formation of AgBr and Ag composite, which was in

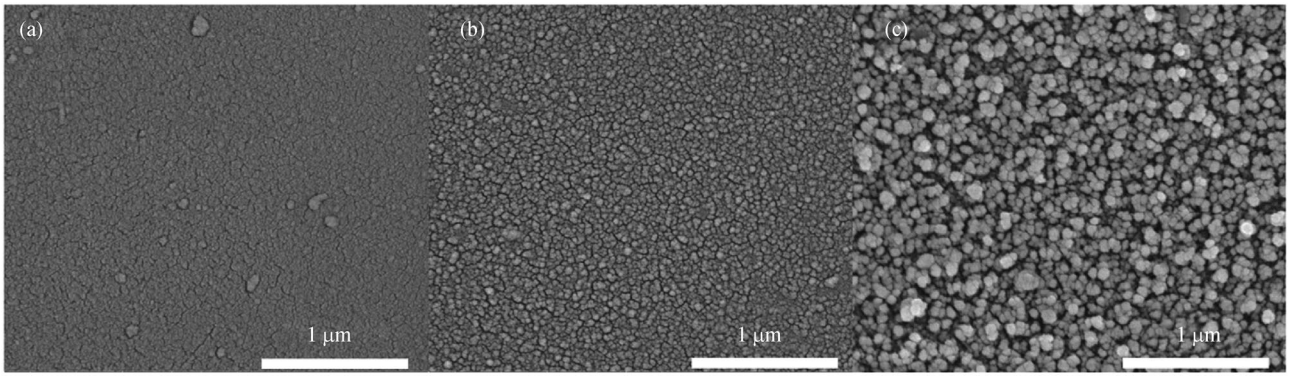

Fig. 1 Surface images of the as-prepared membranes: (a) PAN-ETA, (b) PAN-ETA/CS-TiO_2 and (c) PAN-ETA/CS-TiO_2/Ag-AgBr.

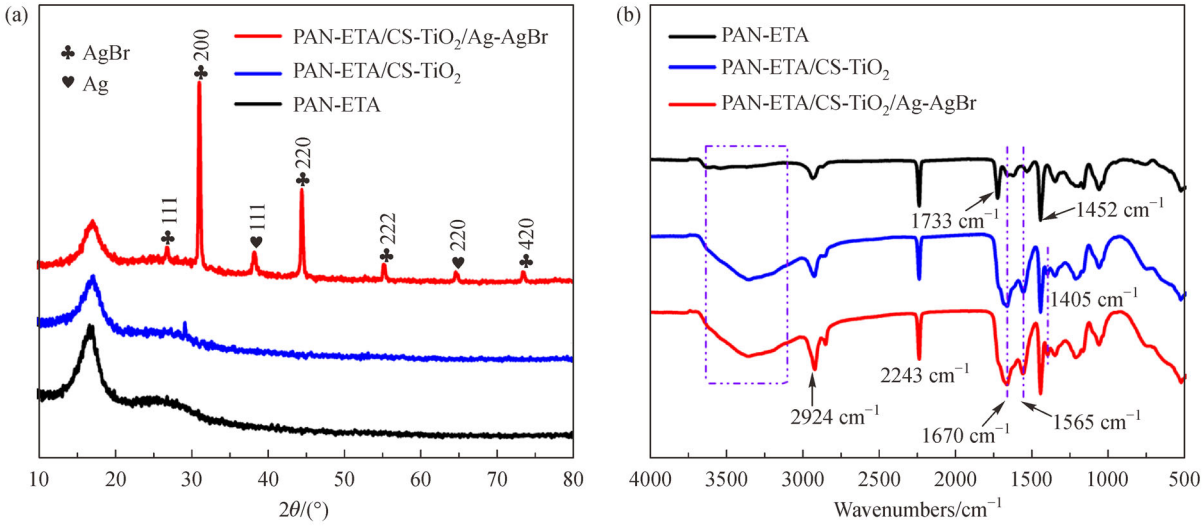

Fig. 2 (a) XRD patterns and (b) ATR-FTIR spectra of the as-prepared membrane.

accordance with the SEM of PAN-ETA/CS-TiO_2/Ag-AgBr [30,39]. Specifically, two peaks appear at 2θ = 38.1° and 64.6°, ascribed to the face-centered cubic Ag (111) and (220) planes, respectively (JCPDS Card, No. 65-2871). Five strong diffraction peaks are also presented at 2θ = 27.0°, 31.0°, 44.3°, 55.0° and 73.3°, which can be indexed to AgBr (111), (200), (220), (222), and (420) plane reflections (JCPDS card, No. 06-0438), respectively.

As shown in Fig. 2(b), two typical peaks, 2243 and 1733 cm^{-1}, appeared for the PAN-ETA membrane, which correspond to the stretching vibration of cyano groups (C≡N) and carbonyl groups (C = O), respectively [40]. The absorption peaks at 2924 and 1452 cm^{-1} correspond to the stretching vibration and bending vibration of $–CH_2$ groups. After filtration of CS-TiO_2 suspension, the peak at 3353 cm^{-1}, which is attributed to the stretching vibration of $–NH_2$ and –OH, was seen for PAN-ETA/CS-TiO_2. The stretching vibration of $–NH_2$ occurs at 1405 cm^{-1}, and the peak at 1565 cm^{-1} corresponding to the C = N group indicates that CS has been crosslinked with GA through the Schiff-Base reaction [41–43]. That would mean crosslinking networks can fix TiO_2 tightly. The absorption peaks of C = O shifted to 1670 cm^{-1} and resulted in a significant enhancement, which suggests the –OH groups reacted with the aldehyde groups. Moreover, it was reported that the interaction between TiO_2 and C = O groups would also give rise to a red shift for the C = O groups [13,44]. Compared to the CS-TiO_2 decorated membrane, the absorption spectrum of the Ag-AgBr modified membrane showed no distinct difference.

XPS analysis was performed as shown in Fig. 3. Characteristic peaks of C 1s, N 1s and O 1s were detected in the XPS survey spectra of all membranes (Fig. 3(a)). After vacuum filtration of the CS-TiO_2 suspension, an obvious signal of Ti 2p was found, which demonstrated the successful introduction of TiO_2 on the membrane surface. For the PAN-ETA/CS-TiO_2/Ag-AgBr membrane, the Ag 3d and Br 3d XPS spectra appeared, which illustrates that AgBr and Ag nanoparticles were spatially distributed on the membrane surface. To further determine the states of

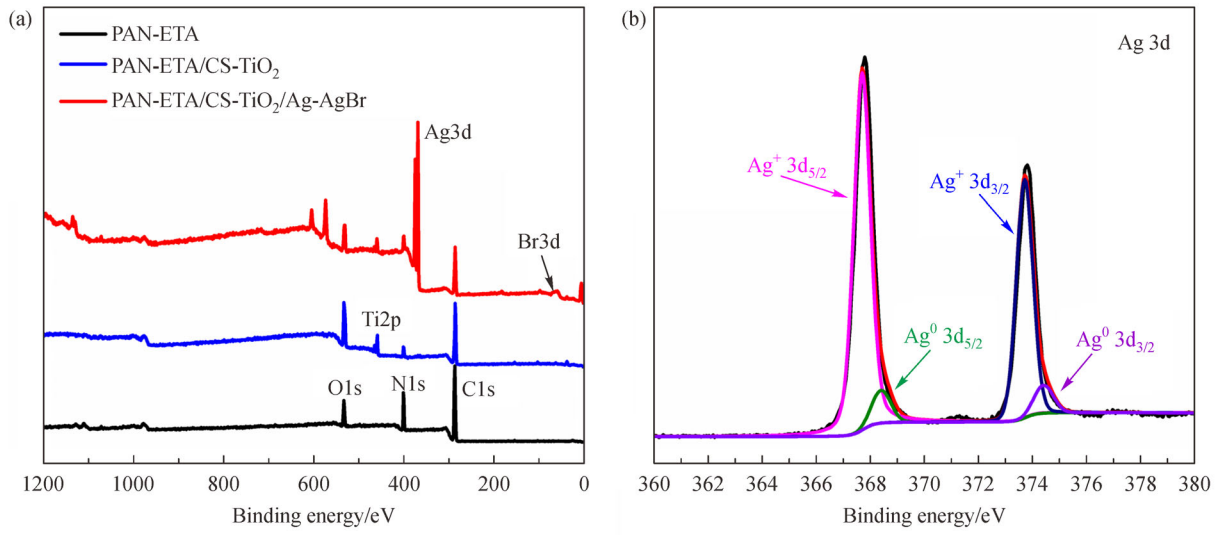

Fig. 3 (a) XPS survey of the as-prepared membranes and (b) Ag 3d high resolution spectra.

Ag, the Ag 3d XPS spectrum was measured as shown in Fig. 3(b). The Ag 3d5/2 and Ag 3d3/2 peaks can be fitted to two sets of peaks, in which the set of peaks at 367.7 and 373.7 eV is assigned to Ag^+ in AgBr while that at 368.4 and 374.4 eV belongs to metallic Ag [30,45–47]. According to the peak areas in XPS, the relative contents of metallic Ag and Ag^+ in the total Ag were calculated to be 9.72 at-% and 90.28 at-%, respectively, further illustrating the coexistence of Ag and AgBr in the PAN-ETA/CS-TiO_2/Ag-AgBr membrane.

The water contact angle is adopted to evaluate the relative surface hydrophilicity of the membranes. Generally, a smaller contact angle displays better hydrophilicity [26]. As shown in Fig. 4, the pristine PAN-ETA membrane exhibits the highest contact angle of 76.5°, corresponding to the lowest surface hydrophilicity. After filtration of CS-TiO_2 solution, the hydrophilicity of the PAN-ETA/CS-TiO_2 membrane is significantly improved due to the amount of hydroxyl groups on the membrane surface. This result should also be ascribed to the embedded TiO_2 nanoparticles on the membrane surface. The loading of Ag-AgBr nanoparticles had no distinct influence on the hydrophilicity of the PAN-ETA/CS-TiO_2/Ag-AgBr membrane, and a slightly higher contact angle was obtained resulting from part of hydrophilic TiO_2 being covered by Ag-AgBr nanoparticles.

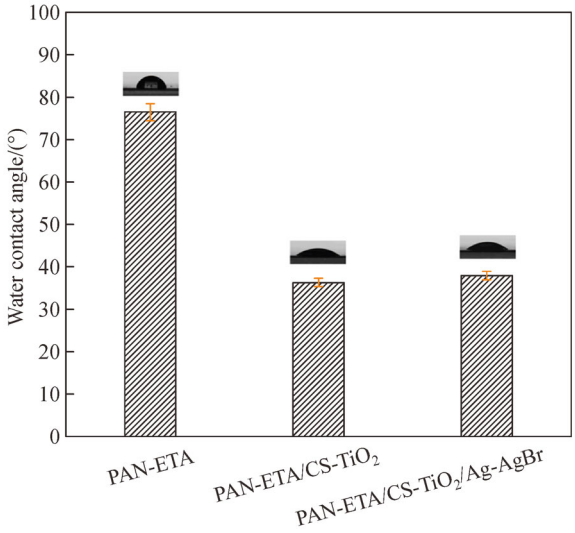

Fig. 4 Water contact angle of the as-prepared membrane.

3.2 Dye rejection performance of membrane

The dye rejections of the as-prepared membrane were tested and the results are summarized in Fig. 5. In view of the PAN-ETA membrane (Fig. 5(a)), the water flux reached ~120 $L \cdot m^{-2} \cdot h^{-1} \cdot bar^{-1}$ and the rejection of MO was comparatively low, only 29.12%. After filtration of CS solution, the water permeability reduced to 41.64 $L \cdot m^{-2} \cdot h^{-1} \cdot bar^{-1}$. Both MB and MO rejections increased from 76.25% to 98.75% and from 29.12% to 91.67%, respectively. The CS layer gives great resistance to water and dye molecules, and simultaneously, it causes decreased water flux and increased rejections of dyes. When the TiO_2 nanoparticles were introduced, the water permeability was found to be enhanced to 54.50 $L \cdot m^{-2} \cdot h^{-1} \cdot bar^{-1}$, followed by slightly declined dye rejections. This may be explained by the improved membrane surface hydrophilicity and the loose structure with nano-voids after incorporation of CS and TiO_2. In addition, the Ag-AgBr decorated membrane can retain high MB rejection of 97.41% and MO rejection of 88.22% similar to the PAN-ETA/CS-TiO_2 membrane, yet a slight loss of water flux was examined due to the increased steric hindrance [13]. Five various dyes, i.e., MB, MO, VB, CR and RB, were tested to further evaluate the performance of PAN-ETA/CS-TiO_2/Ag-AgBr mem-

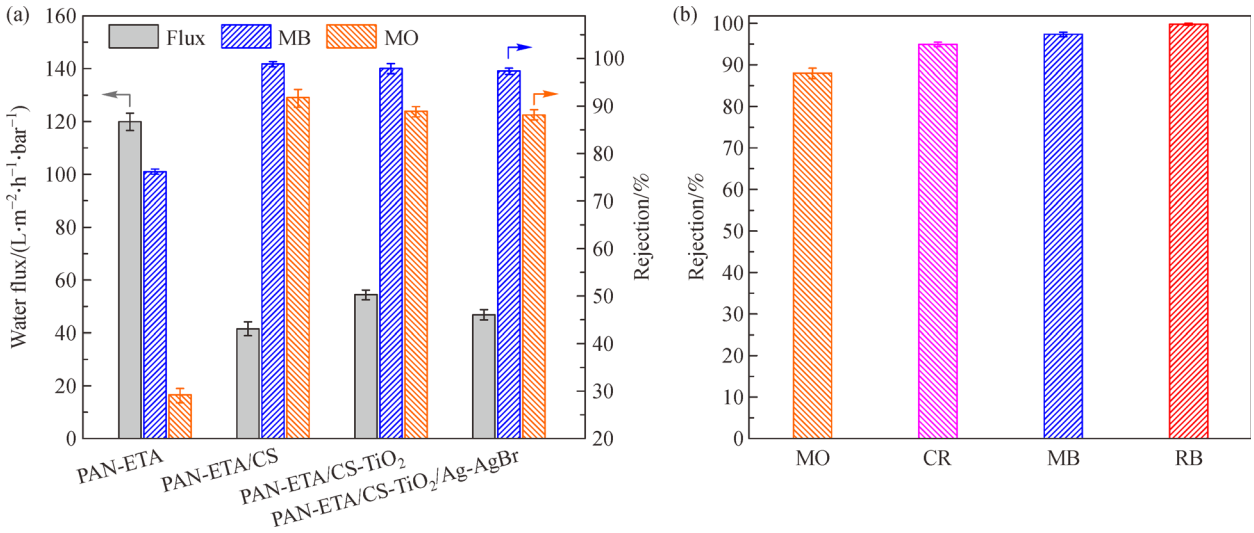

Fig. 5 (a) Water flux and dye rejection of the as-prepared membranes; (b) Various dyes rejection of the PAN-ETA/CS-TiO_2/Ag-AgBr membrane.

brane. As presented in Fig. 5(b), the rejections of negatively charged dyes (MO, CR, MB and RB) increased from 88.22% to 99.98% with the increase of molecular weight (Table S1, cf. Electronic Supplementary Material, ESM).

The MB (100 $mg \cdot L^{-1}$)/NaCl (100 $mg \cdot L^{-1}$) mixture solution was chosen to explore the stability of the PAN-ETA/CS-TiO_2/Ag-AgBr membrane. Figure 6 shows the time-dependent water flux and rejection of MB and NaCl, which revealed that MB and NaCl rejections exhibited no obvious fluctuation while the water permeability decreased slightly (from ~47 to ~45 $L \cdot m^{-2} \cdot h^{-1} \cdot bar^{-1}$). This reduction was reasonable due to MB contamination. Despite a slight drop of flux, the composite membranes exhibited potential long-term stability for dye/salt separation application (dye rejection: ~97%; salt rejection: ~6.5%), benefiting from

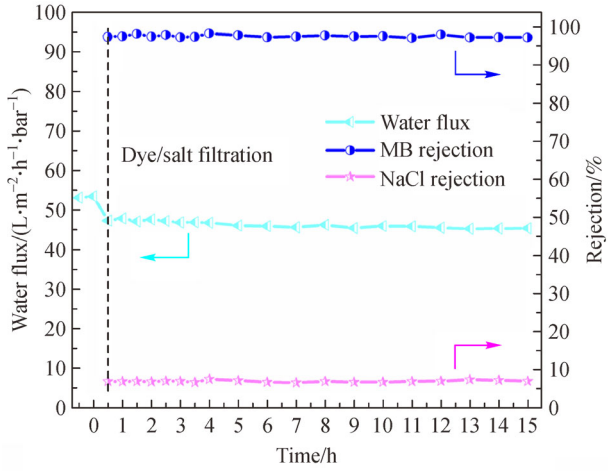

Fig. 6 Long-time stability of the PAN-ETA/CS-TiO_2/Ag-AgBr membrane.

their excellent structural stability and anti-fouling ability. This further proved that the method to bind Ag-AgBr photocatalyst via the CS-TiO_2 layer on PAN-ETA membrane is feasible.

3.3 Photocatalysis properties of PAN-ETA/CS-TiO_2/Ag-AgBr

As presented in Fig. 7, RhB and MEB were chosen to evaluate the photodegradation performance of PAN-ETA/CS-TiO_2/Ag-AgBr photocatalytic membrane under visible light irradiation. After irradiation with visible light for about 30 min, the MEB and RhB solutions with the membrane were degraded almost completely (Fig. 8), while the color of the dye solution without the membrane showed no significant change (Fig. S1, cf. ESM).

The photocatalytic adsorption-degradation efficiency (Fig. 8(a)) of RhB and MEB dyes was obtained with or without the PAN-ETA/CS-TiO_2/Ag-AgBr membrane. In Fig. 8(b), the first-order kinetic equation was used to fit the kinetic of RhB and MEB degradation. The photocatalytic reaction rate constant (k) was 0.11924 and 0.08828 min^{-1} for RhB and MEB, respectively. It can be seen in Fig. 8(c) that the photodegradation of RhB and MEB reached 96.81% and 90.75%, respectively. After going through five cycles, small changes were observed in the photocatalytic performance (Fig. 8(d)), which may be partly attributed to the loss of photocatalyst during the washing process. Compared to other photocatalytic membranes (Table 1), the PAN-ETA/CS-TiO_2/Ag-AgBr membrane shows a comparable degradation capacity for various dyes. These results are due to the existence of Ag-AgBr as a photocatalyst on the membranes.

The degradation mechanism could be illustrated in Fig. 9. Under visible light irradiation, the electron-hole

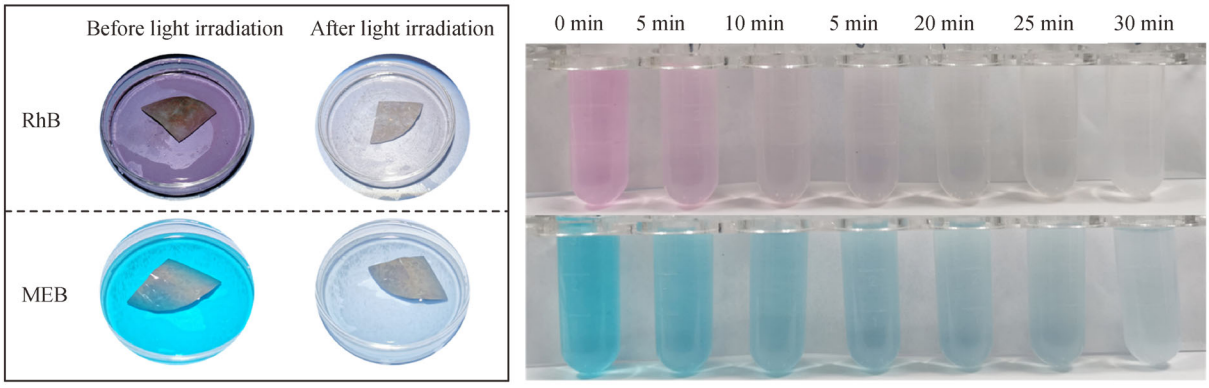

Fig. 7 The color change of RhB and MB solutions under photocatalysis using the PAN-ETA/CS-TiO_2/Ag-AgBr membrane with time from 0 min to 30 min.

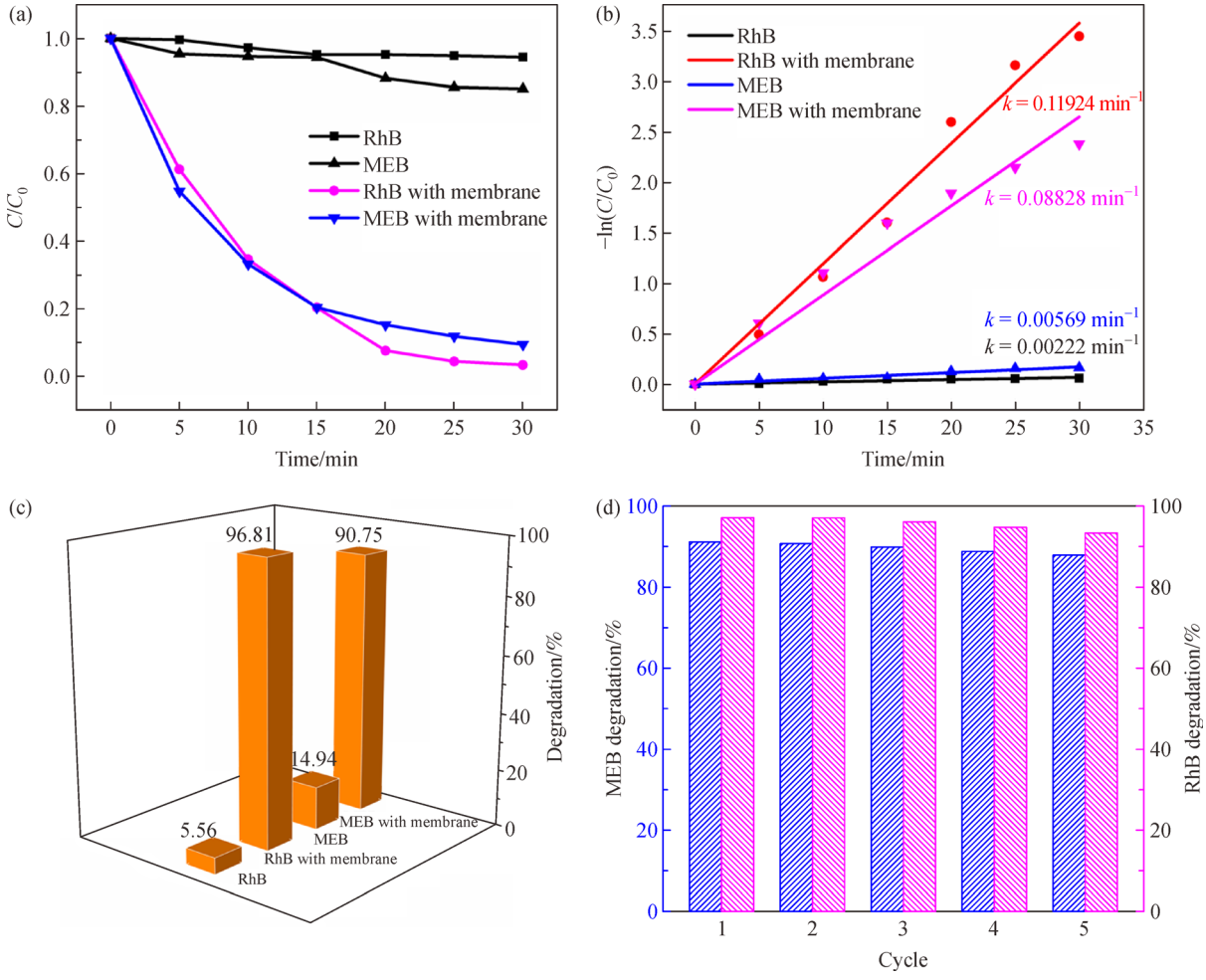

Fig. 8 (a) Plots of dyes degradation efficiency vs. irradiation time; (b) the corresponding kinetic linear simulation curves; (c) degradation performance (%) and (d) recycle degradation efficiency (%).

pairs are easily produced in Ag and AgBr nanoparticles. Then, the motivated electrons and holes transfer from Ag to the conduction band (CB) and the valence bands (VBs), respectively. Subsequently, the electrons on AgBr CB would be captured by O_2 to produce $\bullet O_2^-$ radical, while the holes on AgBr VB would react with Br^- and H_2O to

Table 1 Comparison of the photodegradation performance of different membranes

Membrane	Degradation condition		Irradiation condition	Degradation efficiency	Ref.
	Membrane area	Dye solution volume (concentration)			
PVDF@$CuFe_2O_4$	10 cm^2	50 mL MB (100 mg/L)	Vis, 30 min	99%	[16]
PDA/RGO/Ag_3PO_4/PVDF	36 cm^2	100 mL MEB (20 mg/L)	Vis, 480 min	96.8%	[48]
PVDF/GO/ZnO	9 cm^2	60 mL MEB (10 mg/L)	Vis, 100 min	86.8%	[49]
ZnO/PAN nanofiber	50 mg	10 mL MEB (10 mg/L)	Vis, 480 min	96%	[50]
Ag/TiO_2/PVDF	–	30 mL MEB (10 mg/L)	Vis, 100 min	51%	[51]
Ag/g-C_3N_4/PES	20 cm^2	50 mL MO (10 mg/L)	Vis, 100 min	77%	[52]
PS/CCA/TiO_2	25 cm^2	100 mL RhB (10 mg/L)	Vis, 180 min	82.4%	[53]
Pluronic-TiO_2	–	12 mL RhB (100 μmol/L)	UV, 480 min	90%	[54]
PAN-ETA/CS-TiO_2/Ag-AgBr	4 cm^2	20 mL RhB (10 mg/L) 20 mL MEB (10 mg/L)	Vis, 30 min	96.81% 90.75%	This work

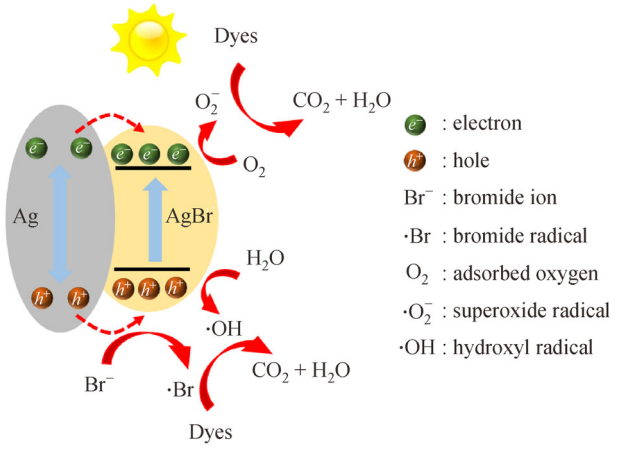

Fig. 9 Possible photocatalytic degradation mechanism of dye pollutants over Ag-AgBr nanoparticles under visible light irradiation.

produce •Br and •OH radicals. The holes, $•O_2^-$, •Br, and •OH radicals degrade MB and RhB dyes into a colorless solution.

4 Conclusions

In this work, PAN-ETA and composite membranes were successfully prepared via facile processes. The introduction of CS and TiO_2 improved membrane surface hydrophilicity, which enhanced dye rejection. In order to obtain anti-fouling and self-cleaning performance, PAN-ETA/CS-TiO_2/Ag-AgBr photocatalytic membranes were fabricated by an *in-situ* partial reduction method. These membranes exhibited excellent dye rejection (MO: 88.22%; CR: 95%; MB: 97.41%; RB: 99.98%) and dye/salt mixture separation efficiency (dye rejection: ~97%; salt rejection: ~6.5%). Especially, the photocatalytic membranes could degrade dye solution under visible light irradiation, which shows potential in regeneration and reuse of the designed membranes.

Acknowledgements We gratefully acknowledge the financial support from the National Natural Science Foundation of China (Grant No. 21908054).

Electronic Supplementary Material Supplementary material is available in the online version of this article at https://doi.org/10.1007/s11705-020-2011-0 and is accessible for authorized users.

References

1. Dong C, Lu J, Qiu B, Shen B, Xing M, Zhang J. Developing stretchable and graphene-oxide-based hydrogel for the removal of organic pollutants and metal ions. Applied Catalysis B: Environmental, 2018, 222: 146–156
2. Liu H, Sun R, Feng S, Wang D, Liu H. Rapid synthesis of a silsesquioxane-based disulfide-linked polymer for selective removal of cationic dyes from aqueous solutions. Chemical Engineering Journal, 2019, 359: 436–445
3. Khalil A, Aboamera N M, Nasser W S, Mahmoud W H, Mohamed G G. Photodegradation of organic dyes by PAN/SiO_2-TiO_2-NH_2 nanofiber membrane under visible light. Separation and Purification Technology, 2019, 224: 509–514
4. Zhao Y, Kang S, Qin L, Wang W, Zhang T, Song S, Komarneni S. Self-assembled gels of Fe-chitosan/montmorillonite nanosheets: Dye degradation by the synergistic effect of adsorption and photo-Fenton reaction. Chemical Engineering Journal, 2020, 379: 122322
5. Samanta P, Chandra P, Desai A V, Ghosh S K. Chemically stable microporous hyper-cross-linked polymer (HCP): an efficient selective cationic dye scavenger from an aqueous medium. Materials Chemistry Frontiers, 2017, 1(7): 1384–1388
6. Verma A K, Dash R R, Bhunia P. A review on chemical coagulation/flocculation technologies for removal of colour from textile wastewaters. Journal of Environmental Management, 2012, 93(1): 154–168
7. Dutta K, Mukhopadhyay S, Bhattacharjee S, Chaudhuri B.

Chemical oxidation of methylene blue using a Fenton-like reaction. Journal of Hazardous Materials, 2001, 84(1): 57–71
8. Zeng G, He Y, Zhan Y, Zhang L, Pan Y, Zhang C, Yu Z. Novel polyvinylidene fluoride nanofiltration membrane blended with functionalized halloysite nanotubes for dye and heavy metal ions removal. Journal of Hazardous Materials, 2016, 317: 60–72
9. Fan H, Gu J, Meng H, Knebel A, Caro J. High-flux membranes based on the covalent organic framework COF-LZU1 for selective dye separation by nanofiltration. Angewandte Chemie International Edition, 2018, 57(15): 4083–4087
10. Liu A, Wang C C, Wang C Z, Fu H F, Peng W, Cao Y L, Chu H Y, Du A F. Selective adsorption activities toward organic dyes and antibacterial performance of silver-based coordination polymers. Journal of Colloid and Interface Science, 2018, 512: 730–739
11. Dou T, Zang L, Zhang Y, Sun Z, Sun L, Wang C. Hybrid g-C_3N_4 nanosheet/carbon paper membranes for the photocatalytic degradation of methylene blue. Materials Letters, 2019, 244: 151–154
12. Brillas E, Martínez-Huitle C A. Decontamination of wastewaters containing synthetic organic dyes by electrochemical methods. An updated review. Applied Catalysis B: Environmental, 2015, 166-167: 603–643
13. Li J, Yuan S, Zhu J, Van der Bruggen B. High-flux, antibacterial composite membranes via polydopamine-assisted PEI-TiO_2/Ag modification for dye removal. Chemical Engineering Journal, 2019, 373: 275–284
14. Li B, Meng M, Cui Y, Wu Y, Zhang Y, Dong H, Zhu Z, Feng Y, Wu C. Changing conventional blending photocatalytic membranes (BPMs): focus on improving photocatalytic performance of Fe_3O_4/g-C_3N_4/PVDF membranes through magnetically induced freezing casting method. Chemical Engineering Journal, 2019, 365: 405–414
15. Zhu J, Wang J, Hou J, Zhang Y, Liu J, Van der Bruggen B. Graphene-based antimicrobial polymeric membranes: a review. Journal of Materials Chemistry. A, Materials for Energy and Sustainability, 2017, 5(15): 6776–6793
16. Wang T, Wang Z, Wang P, Tang Y. An integration of photo-Fenton and membrane process for water treatment by a PVDF@$CuFe_2O_4$ catalytic membrane. Journal of Membrane Science, 2019, 572: 419–427
17. Ong C S, Goh P S, Lau W J, Misdan N, Ismail A F. Nanomaterials for biofouling and scaling mitigation of thin film composite membrane: a review. Desalination, 2016, 393: 2–15
18. Kochkodan V, Hilal N. A comprehensive review on surface modified polymer membranes for biofouling mitigation. Desalination, 2015, 356: 187–207
19. Athanasekou C P, Moustakas N G, Morales-Torres S, Pastrana-Martínez L M, Figueiredo J L, Faria J L, Silva A M T, Dona-Rodriguez J M, Romanos G E, Falaras P. Ceramic photocatalytic membranes for water filtration under UV and visible light. Applied Catalysis B: Environmental, 2015, 178: 12–19
20. Mozia S, Darowna D, Orecki A, Wróbel R, Wilpiszewska K, Morawski A W. Microscopic studies on TiO_2 fouling of MF/UF polyethersulfone membranes in a photocatalytic membrane reactor. Journal of Membrane Science, 2014, 470: 356–368
21. Gao Y, Hu M, Mi B. Membrane surface modification with TiO_2-graphene oxide for enhanced photocatalytic performance. Journal of Membrane Science, 2014, 455: 349–356
22. Horovitz I, Avisar D, Baker M A, Grilli R, Lozzi L, Di Camillo D, Mamane H. Carbamazepine degradation using a *N*-doped TiO_2 coated photocatalytic membrane reactor: influence of physical parameters. Journal of Hazardous Materials, 2016, 310: 98–107
23. Rawindran H, Lim J W, Goh P S, Subramaniam M N, Ismail A F, Radi bin Nik M Daud N M, Rezaei-Dasht Arzhandi M. Simultaneous separation and degradation of surfactants laden in produced water using PVDF/TiO_2 photocatalytic membrane. Journal of Cleaner Production, 2019, 221: 490–501
24. Hu C, Wang M S, Chen C H, Chen Y R, Huang P H, Tung K L. Phosphorus-doped g-C_3N_4 integrated photocatalytic membrane reactor for wastewater treatment. Journal of Membrane Science, 2019, 580: 1–11
25. Qu L, Zhu G, Ji J, Yadav T P, Chen Y, Yang G, Xu H, Li H. Recyclable visible light-driven O-g-C_3N_4/graphene oxide/N-carbon nanotube membrane for efficient removal of organic pollutants. ACS Applied Materials & Interfaces, 2018, 10(49): 42427–42435
26. Qin A, Li X, Zhao X, Liu D, He C. Engineering a highly hydrophilic PVDF membrane via binding TiO_2 nanoparticles and a PVA layer onto a membrane surface. ACS Applied Materials & Interfaces, 2015, 7(16): 8427–8436
27. Li W, Li B, Meng M, Cui Y, Wu Y, Zhang Y, Dong H, Feng Y. Bimetallic Au/Ag decorated TiO_2 nanocomposite membrane for enhanced photocatalytic degradation of tetracycline and bactericidal efficiency. Applied Surface Science, 2019, 487: 1008–1017
28. Tian J, Hao P, Wei N, Cui H, Liu H. 3D Bi_2MoO_6 nanosheet/TiO_2 nanobelt heterostructure: enhanced photocatalytic activities and photoelectochemistry performance. ACS Catalysis, 2015, 5(8): 4530–4536
29. Liu B, Liu L M, Lang X F, Wang H Y, Lou X W, Aydil E S. Doping high-surface-area mesoporous TiO_2 microspheres with carbonate for visible light hydrogen production. Energy & Environmental Science, 2014, 7(8): 2592–2597
30. Kong W, Wang S, Wu D, Chen C, Luo Y, Pei Y, Tian B, Zhang J. Fabrication of 3D sponge@AgBr-AgCl/Ag and tubular photoreactor for continuous waste water purification under sunlight irradiation. ACS Sustainable Chemistry & Engineering, 2019, 7 (16): 14051–14063
31. Wang P, Huang B, Zhang X, Qin X, Dai Y, Wang Z, Lou Z. Highly efficient visible light plasmonic photocatalysts Ag@Ag(Cl,Br) and Ag@AgCl-AgI. ChemCatChem, 2011, 3(2): 360–364
32. Madaeni S S, Ghaemi N. Characterization of self-cleaning RO membranes coated with TiO_2 particles under UV irradiation. Journal of Membrane Science, 2007, 303(1): 221–233
33. Wang Y X, Ma S, Huang M N, Yang H, Xu Z L, Xu Z. Ag NPs coated PVDF@TiO_2 nanofiber membrane prepared by epitaxial growth on TiO_2 inter-layer for 4-NP reduction application. Separation and Purification Technology, 2019, 227: 115700
34. Lee H S, Im S J, Kim J H, Kim H J, Kim J P, Min B R. Polyamide thin-film nanofiltration membranes containing TiO_2 nanoparticles. Desalination, 2008, 219(1): 48–56
35. Wang Y X, Li Y J, Yang H, Xu Z L. Super-wetting, photoactive TiO_2 coating on amino-silane modified PAN nanofiber membranes for high efficient oil-water emulsion separation application. Journal of Membrane Science, 2019, 580: 40–48

36. Zhang X, Wang M, Ji C H, Xu X R, Ma X H, Xu Z L. Multilayer assembled CS-PSS/ceramic hollow fiber membranes for pervaporation dehydration. Separation and Purification Technology, 2018, 203: 84–92
37. Qin Y, Wang Y X, Yang H, Xu Z L. ETA-m-PAN and its composite membrane with high performance prepared by *in situ* modification/NIPS principle. Macromolecular Materials and Engineering, 2019, 304(4): 1800745
38. Dai J, Sun Y, Liu Z. Efficient degradation of tetracycline in aqueous solution by Ag/AgBr catalyst under solar irradiation. Materials Research Express, 2019, 6(8): 085512
39. Wang P, Huang B, Zhang X, Qin X, Jin H, Dai Y, Wang Z, Wei J, Zhan J, Wang S, Wang J, Whangbo M H. Highly efficient visible-light plasmonic photocatalyst Ag@AgBr. Chemistry (Weinheim an der Bergstrasse, Germany), 2009, 15(8): 1821–1824
40. Dai Z W, Wan L S, Xu Z K. Surface glycosylation of polyacrylonitrile ultrafiltration membrane to improve its anti-fouling performance. Journal of Membrane Science, 2008, 325(1): 479–485
41. Wang J, Zhang W, Li W, Xing W. Preparation and characterization of chitosan-poly(vinyl alcohol)/polyvinylidene fluoride hollow fiber composite membranes for pervaporation dehydration of isopropanol. Korean Journal of Chemical Engineering, 2015, 32(7): 1369–1376
42. Beppu M M, Vieira R S, Aimoli C G, Santana C C. Crosslinking of chitosan membranes using glutaraldehyde: effect on ion permeability and water absorption. Journal of Membrane Science, 2007, 301(1): 126–130
43. Vieira R S, Beppu M M. Interaction of natural and crosslinked chitosan membranes with Hg(II) ions. Colloids and Surfaces. A, Physicochemical and Engineering Aspects, 2006, 279(1): 196–207
44. Ye X, Zhou Y, Chen J, Sun Y. Synthesis and infrared emissivity study of collagen-g-PMMA/Ag@TiO_2 composite. Materials Chemistry and Physics, 2007, 106(2): 447–451
45. Dong R, Tian B, Zeng C, Li T, Wang T, Zhang J. Ecofriendly synthesis and photocatalytic activity of uniform cubic Ag@AgCl plasmonic photocatalyst. Journal of Physical Chemistry C, 2013, 117(1): 213–220
46. Zhu M, Chen P, Liu M. Sunlight-driven plasmonic photocatalysts based on Ag/AgCl nanostructures synthesized via an oil-in-water medium: enhanced catalytic performance by morphology selection. Journal of Materials Chemistry, 2011, 21(41): 16413–16419
47. Eswar N K, Katkar V V, Ramamurthy P C, Madras G. Novel AgBr/Ag_3PO_4 decorated ceria nanoflake composites for enhanced photocatalytic activity toward dyes and bacteria under visible light. Industrial & Engineering Chemistry Research, 2015, 54(33): 8031–8042
48. Zhang R, Cai Y, Zhu X, Han Q, Zhang T, Liu Y, Li Y, Wang A. A novel photocatalytic membrane decorated with PDA/RGO/Ag_3PO_4 for catalytic dye decomposition. Colloids and Surfaces. A, Physicochemical and Engineering Aspects, 2019, 563: 68–76
49. Zhang D, Dai F, Zhang P, An Z, Zhao Y, Chen L. The photodegradation of methylene blue in water with PVDF/GO/ZnO composite membrane. Materials Science and Engineering C, 2019, 96: 684–692
50. Zhou Y, Li X, Yu H Y, Hu G L, Yao J M. Facile fabrication of controllable zinc oxide nanorod clusters on polyacrylonitrile nanofibers via repeatedly alternating immersion method. Journal of Nanoparticle Research, 2016, 18(12): 359
51. Li J H, Yan B F, Shao X S, Wang S S, Tian H Y, Zhang Q Q. Influence of Ag/TiO_2 nanoparticle on the surface hydrophilicity and visible-light response activity of polyvinylidene fluoride membrane. Applied Surface Science, 2015, 324: 82–89
52. Zhang M, Liu Z, Gao Y, Shu L. Ag modified g-C_3N_4 composite entrapped PES UF membrane with visible-light-driven photocatalytic antifouling performance. RSC Advances, 2017, 7(68): 42919–42928
53. Mahlambi M M, Mahlangu O T, Vilakati G D, Mamba B B. Visible light photodegradation of Rhodamine B dye by two forms of carbon-covered alumina supported TiO_2/polysulfone membranes. Industrial & Engineering Chemistry Research, 2014, 53(14): 5709–5717
54. Goei R, Dong Z, Lim T T. High-permeability pluronic-based TiO_2 hybrid photocatalytic membrane with hierarchical porosity: fabrication, characterizations and performances. Chemical Engineering Journal, 2013, 228: 1030–1039